Multi-Channel SAR Image Reconstruction using Data of DLR's New DBFSAR Airborne System

Juan Pablo Navarro Castillo [a], Rolf Scheiber [a], Marc Jäger [a], Alberto Moreira [a]
[a] German Aerospace Center (DLR), Microwaves and Radar Institute, Münchener Str. 20, 82334 Oberpfaffenhofen

Abstract

A major challenge facing state-of-the-art spaceborne Synthetic Aperture Radar (SAR) missions is to provide high-resolution wide-swath (HRWS) imagery. The need to keep a low azimuth sampling rate and to achieve in the same time wider swaths is no more a limitation for high resolution SAR systems, if a multichannel sensor is used and the right reconstruction algorithm is implemented. This paper studies the applicability of an existing Digital Beamforming (DBF) reconstruction algorithm to real multichannel X-band data, acquired by the new DLR DBFSAR airborne system. The investigation analyses the impact of the reconstruction on the azimuth ambiguities and also discusses potential areas of improvement to be addressed in future research.

1 Introduction

The requirements for high-resolution spaceborne SAR imaging contrast with those for wide swath imaging. One of them, and the focus of this paper, concerns the Pulse Repetition Frequency (PRF). High resolution SAR systems need to process a wider azimuth bandwidth, which implies the necessity of using a higher azimuth sampling rate, or PRF. Contrary to that, the requirement to cover a broader swath imposes a longer time window length to receive the radar echoes, thus forcing a lower PRF [1].

Multi-channel architectures combined with digital beamforming use the displaced phase centre (DPC) technique to overcome this fundamental limitation, simultaneously achieving high resolution and wide swath SAR images without introducing ambiguities in azimuth [2]. These systems work with aliased receive channels, which operate with a PRF smaller than the processed azimuth bandwidth. As it will be explained briefly in the later sections, the reception of echoes in each channel is followed by a reconstruction stage, where the azimuth ambiguities are cancelled and the recovered image is equivalent to a single channel operating with a PRF N times larger, where N denotes the number of channels arranged in the azimuth direction.

The aim of this paper is to test the reconstruction algorithm proposed in [2] for a monostatic SAR system comprising up to six azimuth channels. First, simulated data with multiple point targets were used in order to test the developed algorithm with a simplified scenario. This was followed by a reconstruction of real acquired data from a measurement campaign of the German Aerospace Center (DLR) DBFSAR airborne system [3], performed in Kaufbeuren in October 2020. In all cases, the data used for the reconstruction were already compressed in range.

The paper is structured as follows: Section 2 presents a quick overview of the basic theory behind the reconstruction algorithm used for the experiments. Section 3 briefly summarises the principal features of the new DLR DBFSAR airborne system and describes the antenna geometry, needed to define the algorithm. Then, the data used for the reconstruction are described and listed in section 4. Afterwards, in section 5, the results for a practical example using three of the six channels is presented. Finally, Section 6 reviews the contents of the paper and compiles some of the potential future investigations and projects where use of these reconstruction techniques is foreseen.

2 Displaced phase centre theory

In this section, a brief summary of the fundamentals of azimuth DBF are presented.

2.1 Multiple signal reception in azimuth

We can define the phase centre of an aperture as the effective position of the transmitted (Tx) or received (Rx) signal, usually placed in the centre of the given aperture. The real position or spacing of the acquired samples in azimuth is taken to be half way between the phase centres of the Tx and Rx antennas [5]. Since the distance between the receiver and transmitter is different for each channel, the real position of a sample will have a displacement with respect to the samples acquired at the same time instant in other channels. Therefore, this basic principle allows for a finer sampling in azimuth when the information in all channels is combined.

2.2 Channel impulse response function

The two-way range history of a multi-channel SAR system is defined in [5] as

$$R_k(t) = r_0(t) + r_0\left(t - \frac{\Delta x_k}{v_s}\right) = r_0(t) + r_k(t), \quad (1)$$

where $r_0(t)$ represents the one-way Tx path and $r_k(t)$ the Rx path. The index k is an integer and will be used from now on as the channel index. v_s is the velocity of the sensor and Δx_k the phase centre separation between transmit and receive. It is assumed that the slant range distance to the target is given by a single function $R_0(t)$ for both Tx and Rx, with a certain azimuth time delay in the latter due to

the displaced phase centre. Taking that into account, the impulse response function (IRF) for one channel can be derived as

$$h_{s,k}(t) \cong h_s(t - \Delta t_k) \cdot e^{j \cdot \Delta\varphi_k}, \quad (2)$$

$$H_{s,k}(f) \approx H_s(f) \cdot e^{j \cdot \Delta\varphi_k} \cdot e^{-j \cdot 2\pi \cdot f \cdot \Delta t_k}$$

$$= H_s(f) \cdot H_k(f)\,, \quad (3)$$

where $h_{s,k}(t)$ and $H_{s,k}(f)$ denote the IRF in the time domain and in the frequency domain, respectively. This channel IRF is equivalent to the IRF of a conventional monostatic SAR system $h_s(t)$, where the transmitter and the receiver have the same phase centre, after adding a time shift (Δt_k) and a constant phase shift ($\Delta\varphi_k$) [5]. These shifts depend on Δx_k, defined in (1), implying that the value of $H_k(f)$ will be different for each channel, while $H_s(f)$ will be independent of the channel. $H_k(f)$ can be described as the influence of the multi-channel system and will be the key to build the reconstruction chain. There are several approaches to estimate the value of $H_k(f)$ [2,6], depending on the system geometry. The experiments performed in this study use the approach from [2], as it assumes an equivalent monostatic multi-channel system.

2.3 The reconstruction algorithm

The structure of the reconstruction algorithm used, first proposed in [2], and based on the studies presented in [7], is shown within the red box in Figure 1. The block diagram shows each of the aliased channels k = 1...N, to which a filter $P_k(f)$ is applied as a function of the Doppler frequency f. As explained in [2], the filters $P_k(f)$ depend on the PRF and the system geometry, since their value is derived from the inversion of a matrix composed of the functions $H_k(f)$.

After the filtering stage, all the channels are coherently summed, obtaining the signal which will be processed as a conventional range compressed monostatic SAR signal sampled with an azimuth sampling rate of $N \cdot PRF$.

In practice, and depending on the SAR processor used for focusing in azimuth, it can be more convenient to have a reconstructed image that preserves the range history of a specific channel, denoted in this paper as reference channel, whose Rx phase centre does not coincide with Tx. In this case, the relative azimuth distance to the reference channel phase centre becomes the key parameter to define the reconstruction filters. In this scenario, the function $H_k(f)$ for the reference channel will be always

$$H_{ref}(f) = 1\,, \quad (4)$$

so that its phase is kept after the coherent summation with the rest of channels, obtaining at the end the following reconstructed signal:

$$h_{s,ref}(t) \cong h_s\left(t - \Delta t_{ref}\right) \cdot e^{j \cdot \Delta\varphi_{ref}}, \quad (5)$$

where Δt_{ref} and $\Delta\varphi_{ref}$ depend on the distance between Tx and the Rx reference antenna. For more details about the mentioned reconstruction matrices and equations, please refer to [2] or [5].

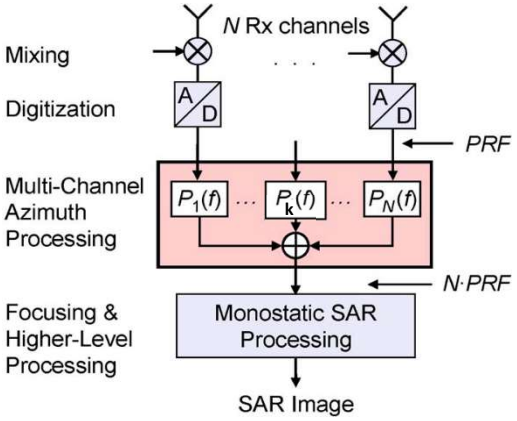

Figure 1 Multi-channel SAR system: block diagram with a DBF azimuth processing network [8].

3 Airborne DBFSAR system

Airborne SAR sensors are essential to research, especially to validate innovative techniques for later implementation on a satellite. Concerning DBFSAR systems, DLR has developed a new high-resolution airborne SAR system with digital beamforming capabilities. This is intended to supplement the operational FSAR airborne sensor [3].

3.1 The DBFSAR antenna array

Previous DBF demonstrations, such as the one presented in [8], were performed using the FSAR airborne DLR sensor. This system used up to four antennas, operated in two receiver chains, meaning that a maximum of two channels could be acquired simultaneously. In contrast, the new DBFSAR airborne sensor can currently use up to six different antennas, which are recorded simultaneously for a total of six receive channels. In addition, there is the possibility to toggle different Tx antennas to introduce different gains and phase centres. Furthermore, the DBFSAR airborne system supports multi-channel Ground Moving Target Indication (GMTI) and Marine MTI (MMTI). In Figure 2, the aircraft used in the campaigns is depicted. Under the image of the airplane, a picture of the antenna array is shown. The Rx channels, delimited by blue squares, each comprise 3 x 2 DBF-Receive Antenna Modules (DBFRAM). The Tx channel is composed of 4 x 3 DBFRAM modules and is coloured in red. The phase centre of each antenna is located roughly in the middle of each DBFRAM group [3].

3.2 DBFSAR sampling

The optimum PRF for a given DBFSAR system is the one which corresponds to a uniform sampling, as explained in [5]. From equation (7), the ideal PRF is

$$PRF_{uni} = \frac{2 \cdot v_s}{N \cdot \Delta x}, \qquad (6)$$

where Δx denotes the along-track displacement between adjacent sub-apertures, which must be constant for uniform sampling.

The spatial sample distribution in azimuth for the experiments described in this paper is illustrated in Figure 3. As will be explained in the next section, the original raw datasets were decimated to generate aliased channels. Furthermore, the subsampling factor was chosen such that a quasi-uniform sampling scenario was obtained. The capability to use this technique with non-uniform sampling cases was demonstrated in [8].

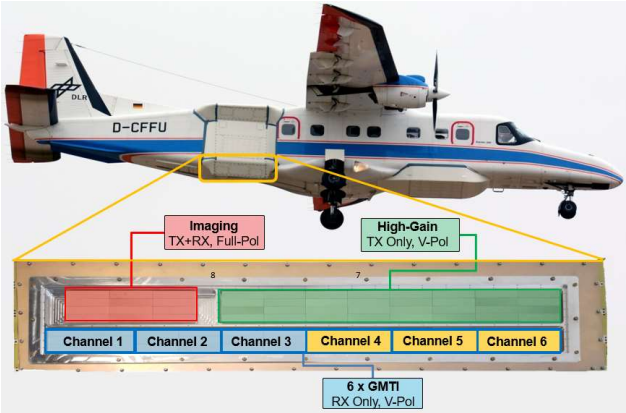

Figure 2 DLR DO 228-212 aircraft showing the location and a zoom of the antenna array. The yellow rectangles correspond to the antennas used for this demonstration.

4 Experimental data

4.1 Input data preparation

A similar procedure as followed in [8] was used to generate the input for the reconstruction. The main difference lies in the motion compensation (MoCo) approach. The relative second order MoCo applied in this experiment is based on the one used in the two-step range dependent motion compensation first suggested in [9]. However, while in [8] MoCo consisted of the correction of each individual channel track to a linear trajectory, the alternative used in this experiment preserved the non-linear motion of the reference channel and adjusted the rest of the channels to the shape of this "reference" trajectory. Furthermore, the motion compensation in [8] was performed before low pass filtering and decimation while, in this case, the relative MoCo is applied after decimation, making the approach applicable to a real subsampled multi-channel airborne system configuration. The term "relative" was used with intention, since a full MoCo is still required when the reference channel is reconstructed.

As in [8], the original dataset was acquired with a high oversampling in the azimuth dimension. In order to show the effectiveness of the reconstruction algorithm, it was necessary to pre-process the input by subsampling the datasets applying a certain factor, denoted as K_{sub}, in order to obtain aliased images. The block diagram describing the process, leading to the reconstructed image, is shown in the top half of Figure 4. There, a filtering stage previous to the decimation can be seen. This low-pass filter (LPF) was just applied to the real data, since, it that case, the data needed an additional subsampling factor, denoted as K_d, to be comparable to the simulated data. For this reason, a filtering proportional to this additional decimation factor (K_d) was required to assure a non-aliased reference case.

In order to quantify the improvement in comparison with a traditional single-channel system, two additional datasets were created. The first one was the output of a single subsampled, and, hence aliased, channel. The last set was the oversampled original dataset. Both were pre-processed in a manner similar data input to the reconstruction process. The block diagrams for these two data sets are presented in the bottom half of Figure 4.

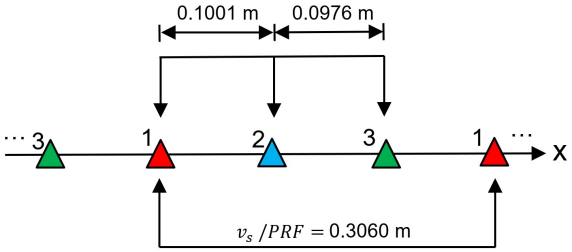

Figure 3 Azimuth spatial sampling for 3 of the 6 channels after decimating the original raw datasets with a subsampling factor of 10 ($PRF = 300$ Hz). The sensor velocity v_s was around 90.3 m/s.

4.2 Simulated data

Before testing the developed algorithm with real data, some simulated scenarios were generated to have a better understanding of the influence of different potential error sources, such as variable sensor velocity, across-track motion or the antenna pattern.

The first dataset included simulated, range-compressed data of ideal trihedral reflector responses. The geometry was basically identical to that of the real data but across-track motion and the antenna pattern were excluded, leaving a system with non-constant, realistic sensor speed. Next, a more realistic simulation included across track motion, but the antenna pattern was still not considered. Finally, the antenna pattern was added to obtain a full featured simulation, very close to what can be expected with the real data.

For the three cases an operational $PRF_{op} \approx 600$ Hz was selected. Then, a subsampling factor $K_{sub} = 2$ was chosen to alias the individual channels, leaving $K_d = 1$. This time, no previous low-pass filtering was required. Since the azimuth bandwidth (B_{az}) was set equal to PRF_{op}, applying a decimation of two reduced the individual channel PRF to 300 Hz resulted in an aliased spectrum. The relevant parameters for the simulated system are listed in Table 1.

4.3 Real data

The last step was to take real range-compressed DBF-SAR data from the measurement campaign in Kaufbeuren

in October 2020 for the tests presented in this paper. As noted above, the real data did not include any new complexity that was not already present in the third simulated dataset.

One significant difference between the real and the simulated data is the high oversampling present in the airborne SAR datasets, as they were used for different purposes besides demonstrating digital beamforming capabilities. An additional decimation factor, denoted K_d in Figure 4, was required in order to obtain a comparable subsampled scenario like the one shown in the simulations.

In this case, the original operational PRF for each channel was approximately PRF_{op}= 3 kHz. For this reason, an additional subsampling factor $K_d = 5$ was included to set an azimuth bandwidth of 600 Hz, and therefore, resulting in a total subsampling factor of $K_{sub} \cdot K_d = 10$. This factor K_d was applied even to the reference dataset, since the aim was to generate the same scenario presented in the simulations. Then, as before, the individual channel PRF was reduced to 300 Hz by decimation, resulting in aliased spectra. The relevant parameters for the system are listed on the right in Table 1.

Parameter	Simulations	DBFSAR Data
Carrier frequency	9.50 GHz	
Chirp bandwidth	400.00 MHz	
Sensor velocity	90.12 m/s	90.33 m/s
Sensor altitude	3050.00 m	
Operational PRF	600.96 Hz	3004.81 Hz
Azimuth bandwidth	600.00 Hz	
Processed Doppler bandwidth	500.00 Hz	
Processed Doppler centroid	-245.58 Hz	-246.18 Hz
Number of channels	3	

Table 1. Important system and processing parameters

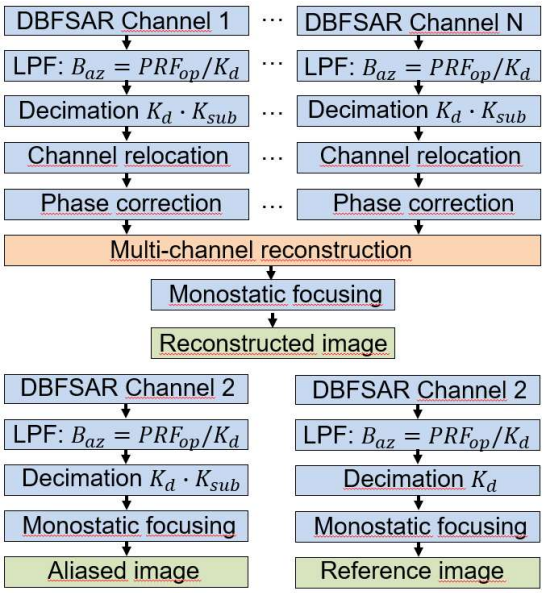

Figure 4 Block diagram summarizing input data generation and SAR processing for different cases: Reconstruction of multi-channel data (top), ideal monostatic reference (bottom right), and image for a single aliased channel (bottom left).

5 Results

5.1 Simulated data reconstruction

In the interest of clarity, a small area of the output of the processor was selected for illustration. In Figure 5, a focused point target in time domain can be observed. This image will be used as reference for all the simulations. The 2D plots in this section show beta naught backscatter amplitudes. For a better representation of the results, the data range covered by the image colormap was reduced by saturating all the values over a certain threshold (vmax). The point target and its 1st order azimuth ambiguities are highlighted by circles, blue and red, respectively. Next to them, their respective original peak values (without applying any plotting threshold) are depicted, expressed in dB. Additionally, in the right corner on the bottom of each image, the azimuth resolution (δ_{az}) achieved for the bandwidth used in the azimuth compression (500 Hz) is depicted.

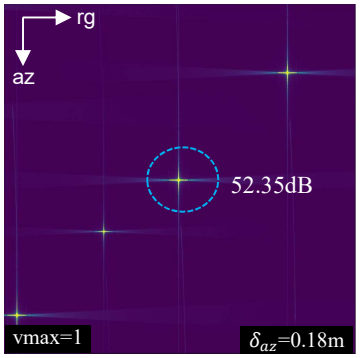

Figure 5 Reference focused simulated point target.

5.1.1 Simulation with only variable sensor velocity

For the first case, the aliased channel is shown on the left of Figure 6, where the ambiguities of the point target are present in the azimuth direction. The right side of Figure 6 shows the image obtained after applying the reconstruction algorithm using the three channels presented in Figure 3.

After reconstruction, the Azimuth Ambiguity to Signal Ratio (AASR) was clearly improved. The considerable difference of energy or asymmetry between both ambiguities, shown on the right plot in Figure 6, is due to non-compensated residual motion errors, e.g. non-constant velocity, during the reconstruction process.

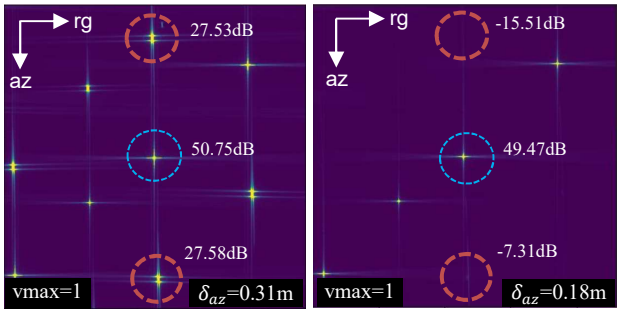

Figure 6 Left: aliased scenario after applying a subsampling factor K_d = 1 and K_{sub}= 2. Right: Reconstructed point target using N = 3 channels.

It is also important to remark, that the reconstruction managed to achieve the same azimuth resolution than the original image (0.18 m), while the single subsampled channel just could reach a resolution of 0.31m.

5.1.2 Simulation with across-track motion

After adding the real aircraft motion to the simulated data, the implementation of the relative MoCo, introduced in Section 4.1, became a mandatory processing step. The result on the left of Figure 7 shows the focused reconstructed signal without relative MoCo. It shows that the AASR did not improve or even got worse. In contrast, after applying the MoCo correction, the ambiguity level was significantly reduced, but artefacts remain discernable.

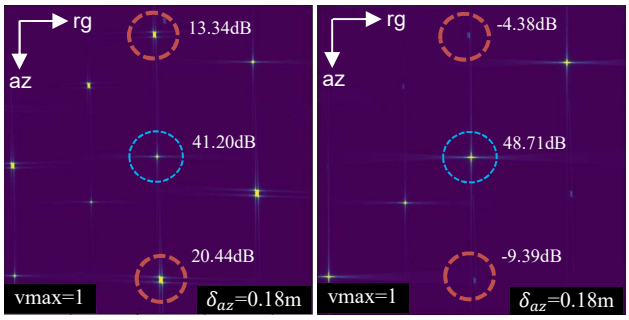

Figure 7 Left: reconstructed image without using the relative MoCo. Right: Reconstructed point targets when applying phase correction before reconstruction. In both cases K_d = 1, K_{sub}= 2 and N = 3.

5.1.3 Simulation with antenna pattern

Including the antenna pattern did not introduce significant additional difficulties. Each channel dataset had its own antenna pattern, and this was not considered during the reconstruction. Adding this to the fact that the antenna pattern itself shaped the spectrum, the level of energy within the whole scene changed, affecting differently to the strength of each ambiguity.

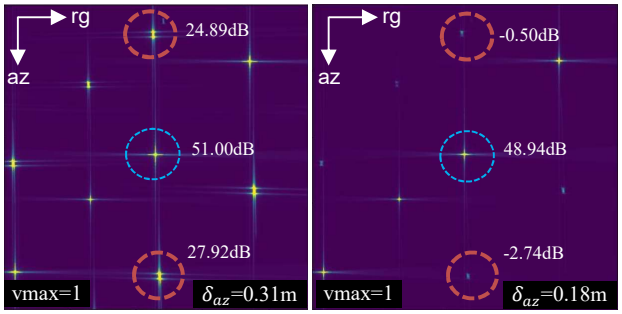

Figure 8 Left: aliased scenario after applying a subsampling factor K_d = 1 and K_{sub}= 2. Right: Reconstructed point targets using N = 3 channels and phase correction before reconstruction.

5.2 DBFSAR data reconstruction

After applying a subsampling factor $K_{sub} \cdot K_d = 10$, to obtain a channel PRF comparable to that of the simulation, the output of the processor is presented in Figure 9. On top, the reference signal without any kind of subsampling and without ambiguities is shown. Then, in the left, the aliased image is illustrated. Finally, the reconstructed image using three channels is plotted on the bottom right. As it can be observed, the ambiguities in the reconstructed image are still present, but the AASR after reconstruction was at least 20dB better than the output of one single channel, reflecting a clear improvement of the SAR image. Furthermore, it can be also be observed, that as it happened with the simulated data, the resolution of the reconstructed image also improved in comparison with an aliased single channel. To give a better impression of the improvement of the image after reconstruction, Figure 10 shows the entire processed scene. The result based on a single subsampled channel scenario is very poorly focused, while the reconstruction achieves a result very close to the reference image.

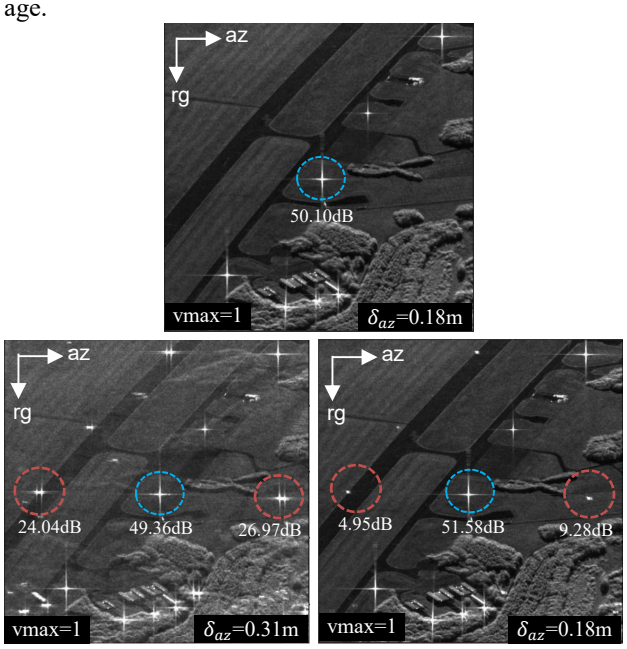

Figure 9 DBFSAR airborne images: (top) reference, (bottom left) aliased and (bottom right) reconstructed zooms.

5.3 Residual ambiguity error sources

The results suggest that in realistic scenarios residual ambiguities remain after the reconstruction. The error sources for these artefacts are currently under study. Nevertheless, it can already be seen that the ambiguous energy in the simulation without across-track motion is significantly lower than in the rest of the experiments. This fact may point towards a non-perfect relative MoCo, entailing residual uncorrected phase errors and increasing residual ambiguities after the coherent summation of channels. These ambiguities are not only not corrected, but also, they may even be amplified by the reconstruction filters. However, this is just a first guess and must be proven in future investigations.

Another important effect to consider is the residual ambiguous energy for a multi-channel system due to the joint antenna characteristic of the Tx and Rx single aperture, since it contains information from azimuth angles that correspond to Doppler frequencies outside the reconstruction band. It is assumed that this effect is negligible in the results, as a filtering of the oversampled data is applied prior to decimation, eliminating these components.

6 Summary and discussion

Before summarizing main points discussed in this paper, a brief look to future research directions for digital beamforming may be of interest to the reader. The results of Section 5 clearly showed that the output from the reconstruction provided an image with much reduced ambiguous energy, but some residual unwanted errors were still evident. Future research might consider additional calibration techniques proposed in [5] and [8] to deal with azimuth ambiguities. On the other hand, the results also suggested that the relative MoCo channel correction used in this experiment was not able to achieve the same performance than the simulation without across-track motion. This should also be further investigated. Finally, for the first experiments, the information of just three of the six system's channels were used, meaning that there are still a lot of unexplored combinations to be tested. For instance, the use of separated groups of channels within the same acquisition to implement interferometry, shall be an interesting area of research.

The aim of all these techniques and experiments is to have a real test scenario that helps to define the system specifications for future spaceborne SAR systems. These are foreseen to use digital beamforming as a technique to achieve high resolution and wide swath acquisitions, simultaneously. Some of the mentioned SAR systems are the ESA missions ROSE-L [4] and Sentinel 1 Next Generation [10], the JAXA mission ALOS-4 [11] and the planned German X-Band spaceborne SAR system HRWS [12].

The results shown in the experiments presented in section 5 demonstrate that the new DLR DBFSAR airborne system has a great potential to perform practical demonstrations for multi-channel processing SAR techniques. Nevertheless, as also mentioned at the beginning of this section, there are still many aspects to test and research.

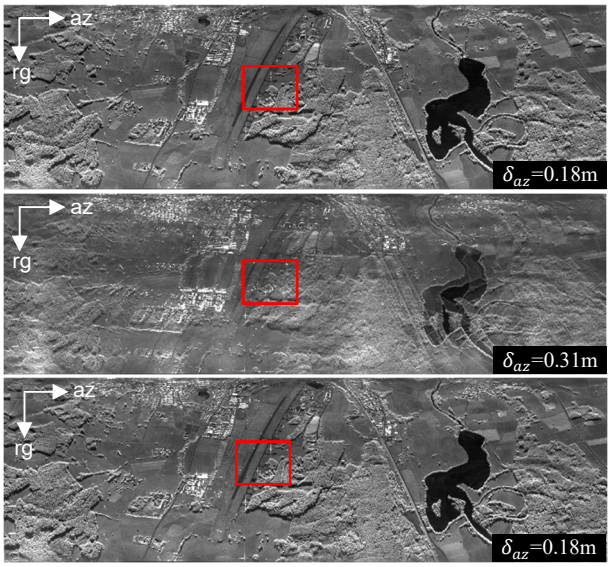

Figure 10: Reference (top), aliased (middle) and reconstructed (bottom) images of an area close to Kaufbeuren, acquired in October 2020 (real size approx. 3 km x 7 km) The red rectangles correspond to Figure 9.

7 Literature

[1] A. Moreira, P. Prats-Iraola, M. Younis, G. Krieger, I. Hajnsek, and K. Papathanassiou, "A Tutorial on Synthetic Aperture Radar," *in IEEE Geoscience and Remote Sensing Magazine* (GRSM), no. 1, pp. 6-43, March 2013

[2] G. Krieger, N. Gebert, and A. Moreira, "Unambiguous SAR signal reconstruction from nonuniform displaced phase center sampling," *IEEE Geoscience and Remote Sensing Letters*, vol. 1, no. 4, pp. 260–264, October 2004

[3] A. Reigber, E. Schreiber, K. Trappschuh, S. Pasch, G. Müller, D. Kirchner, D. Geßwein, S. Schewe, A. Nottensteiner, M. Limbach, A. Schreiber, T. Rommel, R. Horn, M. Jäger, R. Scheiber, S. Baumgartner, S. Joshi, A. Barros Cardoso da Silva, A. Moreira, „The High-Resolution Digital-Beamforming Airborne SAR System DBFSAR," *Remote Sensing* 2020, 12, 1710, May 2020

[4] M. Davidson, N. Gebert and L. Giulicchi, "ROSE-L – The L-band SAR Mission for Copernicus," *EUSAR 2021; 13th European Conference on Synthetic Aperture Radar*, 2021, pp. 1-2.

[5] N. Gebert, G. Krieger, and A. Moreira, "Digital beamforming on receive: Techniques and optimization strategies for high-resolution wide-swath SAR imaging," *IEEE Trans. Aerosp. Electron. Syst.*, vol. 45, no. 2, pp. 564–592, Apr. 2009

[6] N. Sakar, M. Rodriguez-Cassola, P. Prats-Iraola, A. Reigber, A. Moreira, "Analysis of geometrical approximations in signal reconstruction methods for multistatic large along-track baseline SAR constellations," *Proceedings of the 14th European Radar Conference*, pp. 5-8, Oct 2017.

[7] J. Brown, "Multi-channel sampling of low-pass signals," in *IEEE Transactions on Circuits and Systems*, vol. 28, no. 2, pp. 101-106, February 1981.

[8] N. Gebert, F. Queiroz de Almeida and G. Krieger, "Airborne Demonstration of Multichannel SAR Imaging," in *IEEE Geoscience and Remote Sensing Letters*, vol. 8, no. 5, pp. 963-967, Sept. 2011

[9] A. Moreira and Yonghong Huang, "Airborne SAR processing of highly squinted data using a chirp scaling approach with integrated motion compensation," in *IEEE Transactions on Geoscience and Remote Sensing*, vol. 32, no. 5, pp. 1029-1040, Sept. 1994.

[10] D. Geudtner, M. Tossaint, M. Davidson and R. Torres, "Copernicus Sentinel-1 Next Generation Mission," *2021 IEEE International Geoscience and Remote Sensing Symposium IGARSS*, 2021, pp. 874-876.

[11] Motohka, Takeshi, et al. "Overview of ALOS-2 and ALOS-4 L-band SAR," *RadarConf 2021; IEEE Radar Conference*, 2021, pp. 1-4.

[12] M. Bartusch, C. Bruens, A. E. Nuncio Quiroz and S. Stettner, "HRWS: The upcoming German X-Band Spaceborne SAR Mission," *EUSAR 2021; 13th European Conference on Synthetic Aperture Radar*, 2021, pp. 1-4.